


Chern insulating phases and thermoelectric properties of EuO/MgO(001) superlattices

Okan Köksal  and Rossitza Pentcheva ^{*}*Department of Physics and Center for Nanointegration Duisburg-Essen (CENIDE), University of Duisburg-Essen, Lotharstrasse 1, 47057 Duisburg, Germany* (Received 18 May 2020; revised 2 November 2020; accepted 15 December 2020; published 25 January 2021)

The topological and thermoelectric properties of $(\text{EuO})_n/(\text{MgO})_m(001)$ superlattices (SLs) are explored using density functional theory calculations including a Hubbard U term together with Boltzmann transport theory. In $(\text{EuO})_1/(\text{MgO})_3(001)$ SL at the lattice constant of MgO a sizable band gap of 0.51 eV is opened by spin-orbit coupling (SOC) due to a band inversion between occupied localized Eu $4f$ and empty $5d$ conduction states. This inversion between bands of opposite parity is accompanied by a reorientation in the spin texture along the contour of band inversion surrounding the Γ point and leads to a Chern insulator with $C = -1$, also confirmed by the single edge state. Moreover, this Chern insulating phase shows promising thermoelectric properties, e.g., a Seebeck coefficient between 400 and 800 μVK^{-1} . A similar SOC-induced band inversion takes place also in the ferromagnetic semimetallic $(\text{EuO})_2/(\text{MgO})_2(001)$ SL. Despite the vanishing band gap, it leads to a substantial anomalous Hall conductivity with values up to $-1.04 e^2/h$ and somewhat lower Seebeck coefficient. Both cases emphasize the relation between nontrivial topological bands and thermoelectricity also in systems with broken inversion symmetry.

DOI: [10.1103/PhysRevB.103.045135](https://doi.org/10.1103/PhysRevB.103.045135)

I. INTRODUCTION

Recently topological insulators (TIs), that are insulating in the bulk, but have topologically protected conducting edge states with dissipationless charge current at the surface, have attracted a lot of attention in the field of condensed matter physics [1–4]. Several TIs from the V–VI group, e.g., Bi_2Se_3 , Bi_2Te_3 , Sb_2Te_3 are at the same time promising thermoelectric (TE) materials [5–8] that can convert heat into electricity. The connection and common characteristics between TI, in particular Z_2 TIs, which preserve time-reversal symmetry (TRS), and TE, such as heavy elements, narrow band gaps have been recently pointed out [9,10]. In contrast, to our knowledge, Chern insulators—the TRS broken analog of TIs—have received little attention concerning TE applications. Chern insulators are characterized by a nonzero Chern number in the absence of an external magnetic field [11,12]. It is a significant challenge to realize robust Chern insulators. One strategy to achieve breaking of TRS is via doping of magnetic impurities into known topological insulators, such as Mn-doped HgTe -, Cr-, Fe-doped Bi_2Te_3 , Bi_2Se_3 , Sb_2Te_3 [13–15]. Further realization possibilities are $5d$ transition metal atoms on graphene [16,17] as well as OsCl_3 [18].

Transition metal oxides (TMO) with their rich functionality, resulting from the intricate interplay of spin, orbital and lattice degrees of freedom, have a greater tendency towards TRS breaking and larger band gaps compared to conventional sp -bonded systems and are thus an attractive class of materials to search for topologically nontrivial states. Intensive efforts have been directed at finding Chern insulators

in TMO that host a honeycomb lattice, for which Haldane predicted in his seminal work on spinless fermions a quantized anomalous Hall effect [19]. A buckled honeycomb lattice can be formed in (111)-oriented AXO_3 perovskite superlattices (SLs) by two consecutive triangular X layers as proposed by Xiao *et al.* [20]. Several realizations have been proposed, e.g., SrIrO_3 and LaAuO_3 bilayers, however, considering correlation effects resulted in an antiferromagnetic ground state for SrIrO_3 [21,22]. In the $3d$ series, e.g., in $(\text{LaXO}_3)_2/(\text{LaAlO}_3)_4(111)$ SLs [23], LaMnO_3 was identified as a Chern insulator with a band gap of 150 meV when $P321$ symmetry is preserved, but the ground state is a trivial Mott insulator with a Jahn-Teller distortion. Further candidates for quantum anomalous Hall insulators are LaRuO_3 and LaOsO_3 [24], as well as the metastable symmetric ferromagnetic cases of LaPdO_3 , LaPtO_3 , and LaTcO_3 [25,26] honeycomb bilayers encased in $\text{LaAlO}_3(111)$. Corundum-derived SLs provide another realization of the honeycomb lattice. A systematic study of the $3d$ [27], $4d$ and $5d$ [28] series of corundum-based honeycomb layers $(X_2\text{O}_3)_1/(\text{Al}_2\text{O}_3)_5(0001)$ identified the metastable cases of $X = \text{Tc}$, Pt as Chern insulators with $C = -2$ and -1 and band gaps of 54 and 59 meV, respectively.

Other lattice types proposed as candidate Chern insulators are, e.g., rutile-derived heterostructures [29–31], pyrochlore [32], as well as rocksalt-derived superlattices, e.g., EuO/CdO [33] and EuO/GdN SLs [34]. The aim in the latter cases is to combine heavy elements with large SOC in the two initially topologically trivial components in a quantum well (QW) structure and induce a SOC-driven band inversion, analogous to the HgTe/CdTe QW, where band inversion was originally predicted and observed [35–37]. EuO is one of the few ferromagnetically (FM) ordered semiconductors [38] with a Curie temperature (T_C) of 69 K. In both EuO/CdO and EuO/GdN

^{*}Rossitza.Pentcheva@uni-due.de

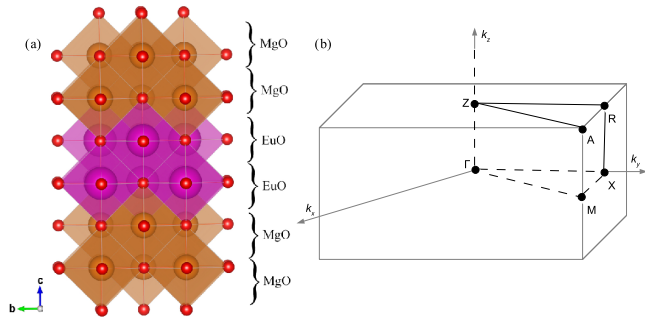


FIG. 1. (a) Schematic view of the $(\text{EuO})_n/(\text{MgO})_m(001)$ superlattice with $n = 2$ and (b) the corresponding Brillouin zone.

the CI state is achieved under considerable compressive strain [33,34]. In EuO/GdN the band inversion involves Eu 4*f* and the Gd 5*d* [34], whereas in EuO/CdO it takes place between the occupied Eu 4*f* and the Cd 5*s* states. The resulting band gap is in the meV range owing to the large $\Delta l = 3$ in the latter case [33].

Here we follow a different strategy: by combining EuO with the large band gap insulator MgO in a $(\text{EuO})_1/(\text{MgO})_3(001)$ superlattice at the lattice constant of MgO (4.21 Å), we achieve a band inversion between Eu 4*f* and 5*d* states within the same component, while MgO merely plays the role of a spacer. We note that despite the large lattice mismatch of 18% between the bulk components EuO/MgO(001) QW heterostructures have already been realized experimentally [39–42] using lattice-matched yttria-stabilized zirconia with the in-plane lattice constant of $a_{\text{EuO}} = 5.14$ Å.

Already Hicks and Dresselhaus [43] proposed that the TE properties of materials can be improved in reduced dimensions as, e.g., in QWs. Experimentally, a giant Seebeck coefficient was reported in δ -doped SrTiO₃ SLs [44]. The confinement- and strain-induced enhancement of TE properties was recently addressed based on first-principles calculations in LaNiO₃/LaAlO₃(001) SLs [45–47] and SrXO₃/SrTiO₃(001) QWs [48], as well as other SrTiO₃-based SLs [49–52]. For example in $(\text{LaNiO}_3)_1/(\text{LaAlO}_3)_1(001)$ [45] the confinement- and strain-induced metal-to-insulator transition at a_{STO} leads to an enhanced in-plane power factor and high Seebeck coefficient. In the following, we discuss the electronic properties of $(\text{EuO})_n/(\text{MgO})_m(001)$ SL shown in Fig. 1 for $n = 2$ and provide topological analysis for the nontrivial cases. Moreover, using Boltzmann transport theory, we address the implications of the topological Chern state in $(\text{EuO})_1/(\text{MgO})_3(001)$ QWs on the thermoelectric properties and compare to the $(\text{EuO})_2/(\text{MgO})_2(001)$ case.

II. THEORETICAL METHODS

Density functional calculations were performed for $(\text{EuO})_n/(\text{MgO})_m(001)$ SLs with the projector augmented wave method [53] as implemented in the VASP [54] code. The cutoff energy of the plane waves was set to 500 eV. For the exchange-correlation functional we used the generalized gradient approximation (GGA) by Perdew, Burke, and Ernzerhof [55]. A Γ -centered k -point grid of $16 \times 16 \times 8$ was adopted

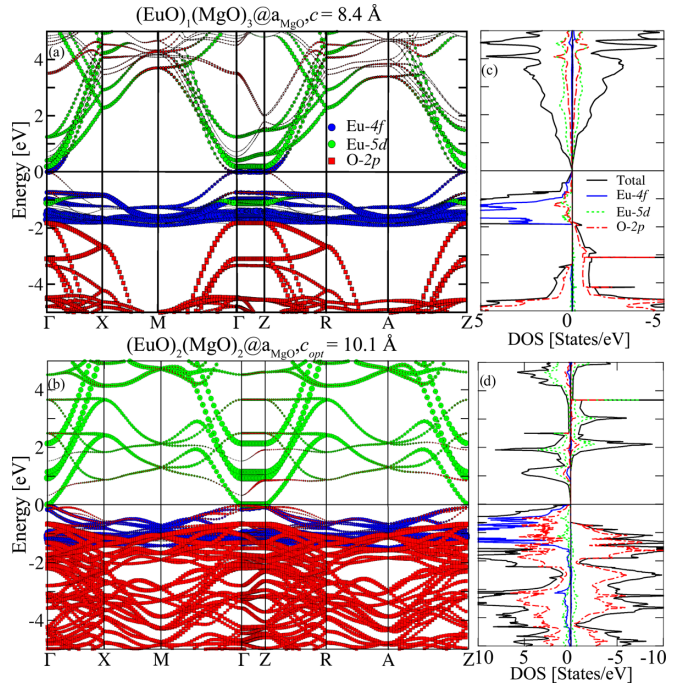


FIG. 2. Element- and orbital-projected band structure of ferromagnetic $(\text{EuO})_n/(\text{MgO})_m(001)$ (a) for $n = 1$ and $m = 3$ with an out-of-plane lattice parameter $c = 2a_{\text{MgO}}$ and (b) for $n = 2$ and $m = 2$ with optimized c . The corresponding projected density of states (DOS) are displayed in (c) and (d), respectively. The orbital character is color coded, highlighting that the states below/above the Fermi level have predominantly Eu-4*f* (blue)/Eu-5*d* (green) as well as O-2*p* (red) character, respectively.

in the self-consistent calculations employing the tetrahedron method [56]. Static electronic correlation effects were taken into account within the GGA +*U* approach in the formulation of Liechtenstein *et al.* [57]. Consistent with previous studies [58–61], an on-site Coulomb repulsion parameter of $U = 7.4$ eV and an exchange interaction parameter $J = 1.1$ eV were considered for the Eu 4*f* states. With these values we obtain a band gap of 1.13 eV for antiferromagnetic coupling, which is in very good agreement with the experimentally reported band gap of 1.12 eV [62] of room-temperature paramagnetic bulk EuO, whereas for the ferromagnetic ground state the band gap amounts to 0.65 eV. The optimized bulk lattice constant of EuO with ferro- and antiferromagnetic arrangement within GGA + *U* is $a = 5.184$ Å and $a = 5.193$ Å, respectively, slightly higher than the experimental value of $a = 5.141$ Å [63]. Similarly, for bulk MgO, GGA yields a bulk lattice parameter of $a = 4.24$ Å, somewhat larger than the experimental lattice constant $a = 4.21$ Å [64–66]. We note that within GGA the band gap of MgO is significantly underestimated (4.28 eV), compared to the experimental value of 7.83 eV [67] and can be improved only by considering many body effects [68,69]. Still the GGA MgO band gap is much larger than the one of the active material EuO, thus the phenomena in the heterostructure are determined by the confined EuO and not affected by the size of the band gap of MgO. The heterostructures were modeled at the experimental lateral lattice constant of MgO and internal parameters were

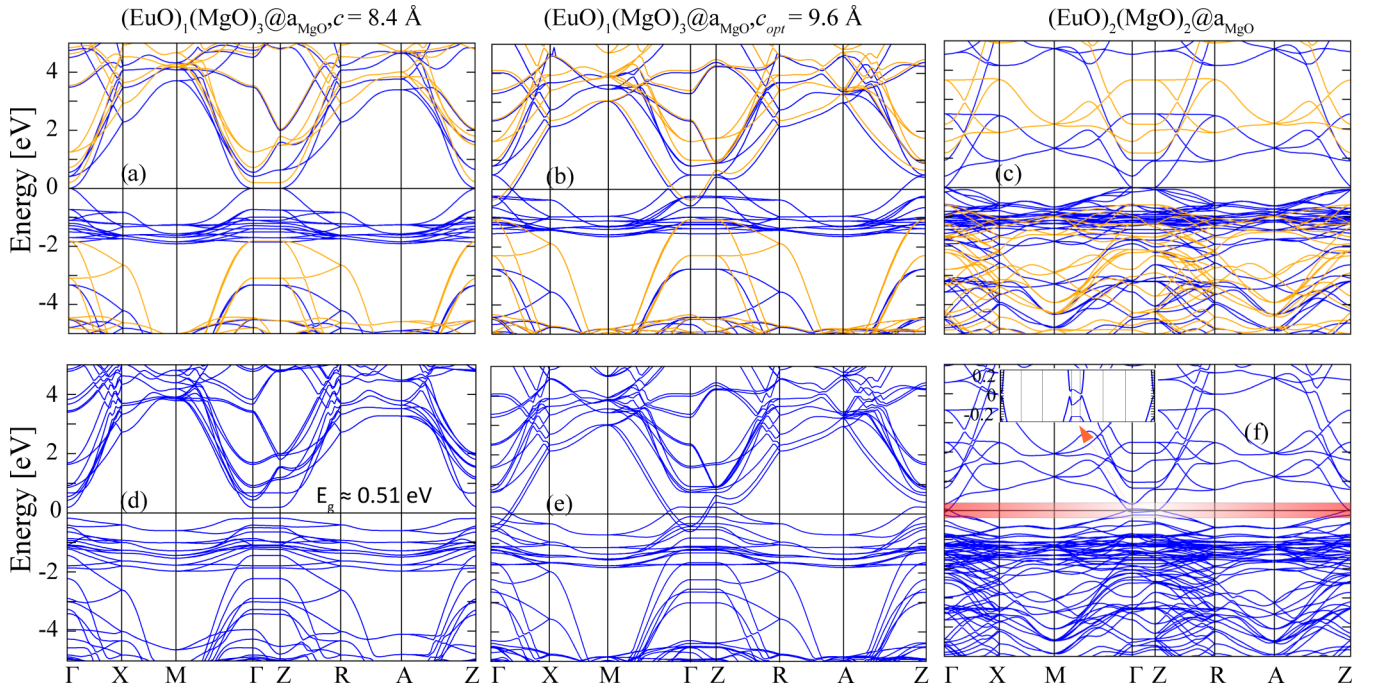


FIG. 3. GGA + U band structures of ferromagnetic $(\text{EuO})_n/(\text{MgO})_m(001)$ at a fixed lateral lattice constant of MgO and (a) constrained or (b) optimized out-of-plane lattice constant c for $n = 1, m = 3$, as well as (c) optimized c for $n = 2, m = 2$. Majority and minority channels are shown in dark blue/light orange. The corresponding GGA + U + SOC band structures are displayed in panels (d)–(f).

relaxed until the Hellman-Feynman forces are less than 1 meV/Å, while the c lattice constant was either fixed at the value of bulk MgO or relaxed. $(\text{EuO})_1/(\text{MgO})_3(001)$ was also explored using the all-electron full-potential linearized augmented plane wave method as implemented in the Wien2k code [70]. The topological analysis, e.g. calculation of the the anomalous Hall conductivity (AHC), was performed using the wannier90 code [71] on a dense k -point mesh of $144 \times 144 \times 12$. The transport coefficients based on input from the density functional theory calculations are obtained within the constant relaxation time approximation using the Boltz-TraP code [72].

III. RESULTS AND DISCUSSION:

A. GGA + U results for $(\text{EuO})_n/(\text{MgO})_m(001)$ quantum wells

In this section we discuss the electronic properties of ferromagnetic $(\text{EuO})_n/(\text{MgO})_m(001)$ superlattices, referred to as (n, m) in the following. According to Hund's rule, Eu^{2+} exhibits a formal $4f^7$ high-spin configuration with a closed shell and a large magnetic moment of $7.05 \mu_B$. The GGA + U element- and orbitally resolved band structure and the spin-dependent projected density of states (DOS) of $(\text{EuO})_1/(\text{MgO})_3(001)$ with c_{MgO} are shown in Figs. 2(a) and 2(c). Just below the Fermi level the band structure is dominated by the narrow (bandwidth ~ 2 eV) half-filled Eu $4f$ bands, whereas the conduction bands are strongly dispersive, e.g., along M- Γ -X and of prevailing Eu $5d$ character [see Fig. 2(a)], respectively. Moreover, the top of the valence and bottom of the conduction band of this quantum well touch along Γ -Z, rendering the system semimetallic with the predominant contribution of majority spin bands. The main effect of the c relaxation is the enhanced dispersion and overlap of

conduction and valence bands along Γ -Z [cf. Fig. 3(b)]. On the other hand, the band structure of $(\text{EuO})_2/(\text{MgO})_2(001)$ with relaxed c [cf. Figs. 2(b) and 3(c)] bears some similarities to $n = 1, m = 3$ at the MgO c lattice constant, in particular, the flat conduction and valence bands touching along Γ -Z, however, exhibits a much stronger overlap and hybridization between the Eu $4f$ and O $2p$ bands and a pronounced O $2p$ contribution along Γ -Z just below the Fermi level, visible also in the orbitally projected DOS in Fig. 2(d).

B. Effect of spin-orbit coupling and topological analysis

Despite similar features in the band structure, the effect of spin-orbit coupling is very distinct for the three systems. The corresponding band structures are displayed in Figs. 3(d)–3(f). While $(\text{EuO})_1/(\text{MgO})_3(001)$ with relaxed c remains metallic with no pronounced rearrangement of bands, for $(\text{EuO})_1/(\text{MgO})_3(001)$ at $c = 2a_{\text{MgO}}$ a significant band gap of 0.51 eV is opened by SOC with out-of-plane magnetization direction. Apparently, the degeneracy of the touching bands at the Fermi level is lifted giving rise to a band inversion along Γ -Z. A band inversion takes place also for $(\text{EuO})_2/(\text{MgO})_2(001)$ with relaxed c but with a vanishing band gap [see inset in Fig. 3(f)]. In order to analyze the origin of the band rearrangement and inversion we plot in Figs. 4(a) and 4(b) the element and orbital projections on the band structure with SOC for (1,3) and (2,2). In contrast to the previously reported band inversion between Eu $4f$ and Cd $5s$ bands in $\text{EuO}/\text{CdO}(001)$ [33] or Eu $4f$ and Gd $5d$ states in EuO/GdN SL [34], for $(\text{EuO})_1/(\text{MgO})_3(001)$ at $c = 2a_{\text{MgO}}$ the band inversion takes place between the $4f$ and $5d$ states of Eu itself. The strong interaction of these bands of opposite parity and $\Delta l = 1$ leads to a substantial band

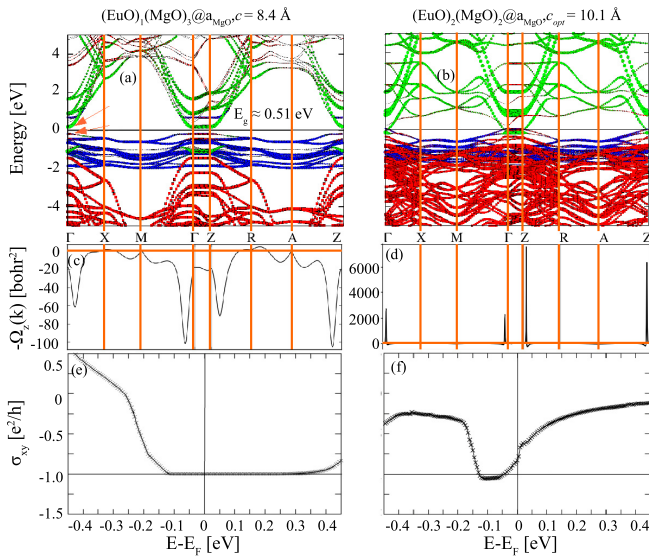


FIG. 4. (a), (b) GGA+ U +SOC band structures for FM $(\text{EuO})_1/(\text{MgO})_3(001)$ and $(\text{EuO})_2/(\text{MgO})_2(001)$ with magnetization along the $[001]$ direction; (c), (d) Berry curvatures along the same k -path. The corresponding anomalous Hall conductivities (AHC) σ_{xy} in units of e^2/h as a function of the chemical potential are displayed in (e), (f).

gap opening. Interestingly, this bears analogy to bulk EuO under pressure, where fluctuations between a $(4f)^7(5d)^0$ and a $(4f)^6(5d)^1$ configuration were suggested in experimental [73] and theoretical studies [74,75]. Upon inclusion of SOC the band structure of $(\text{EuO})_2/(\text{MgO})_2(001)$ with relaxed c shows a reduced contribution of $O\ 2p$ along Γ -Z and a similar inversion of the topmost Eu $4f$ and lowest $5d$ band around E_F , though with a vanishing band gap.

Having identified the origin of the band rearrangement and inversion for the two systems, we proceed to analyze the topological properties. The nontrivial nature of the (1,3) system is underpinned by the Berry curvature [cf. Fig. 4(c)], which exhibits pronounced negative peaks along the Γ -X as well as M - Γ paths, and a flat region along Γ -Z. This leads to the

emergence of a broad plateau in the anomalous Hall conductivity σ_{xy} at E_F in Fig. 4(e), rendering $(\text{EuO})_1/(\text{MgO})_3(001)$ a Chern insulator with a quantized $C = -1$. As shown in Fig. 4(d), sharp peaks arise in the Berry curvature $\Omega(k)$ of $(\text{EuO})_2/(\text{MgO})_2(001)$ at the avoided crossing of Eu $4f$ and $5d$ bands along the M - Γ and Z - R paths with values of 3000 and 8000 bohr^2 . For $(\text{EuO})_2/(\text{MgO})_2(001)$ the Hall conductivity in Fig. 4(f) shows substantial, nearly quantized values ($-1.04 e^2/h$) caused by the nontrivial bands with the plateau being just below E_F and a finite value of $-0.8 e^2/h$ at E_F .

In Fig. 5(a) we plot the spin texture of the relevant bands of $(\text{EuO})_1/(\text{MgO})_3(001)$ at $c = 2a_{\text{MgO}}$ [see Fig. 4(a)]. The occupied band exhibits only positive s_z values throughout the Brillouin zone (BZ). In contrast, the out-of-plane spin component s_z of the lowest unoccupied parabolic band is negative around Γ but reverses sign further away from the BZ center. This switching of spin orientation can be ascribed to the SOC-induced band inversion between the occupied majority $4f$ states and unoccupied minority $5d$ states band along Γ -Z, occurring just above E_F in Fig. 3(a). The surface states shown in Fig. 5(b) using Wanniertools [76] based on the Maximally Localized Wannier functions method presents one topologically protected chiral edge state, connecting the valence and conduction band. In contrast, the edge state for $(\text{EuO})_2/(\text{MgO})_2(001)$ in Fig. 5(c) is obscured due to the overlap of valence and conduction bands along Γ -Z.

C. Thermoelectric properties

In the following, we investigate the thermoelectric properties of the $(\text{EuO})_n/(\text{MgO})_m(001)$ SLs. A central quantity related to the TE efficiency is the figure of merit:

$$ZT = \frac{S^2\sigma}{\kappa}T, \quad (1)$$

where S is the Seebeck coefficient, σ is the conductivity and κ is the thermal conductivity. Since to our knowledge neither experimental nor theoretical values are available in the literature for the lattice thermal conductivity of the QW and even for bulk EuO, we consider here only the electronic part of the thermal conductivity, which can be expressed as the second

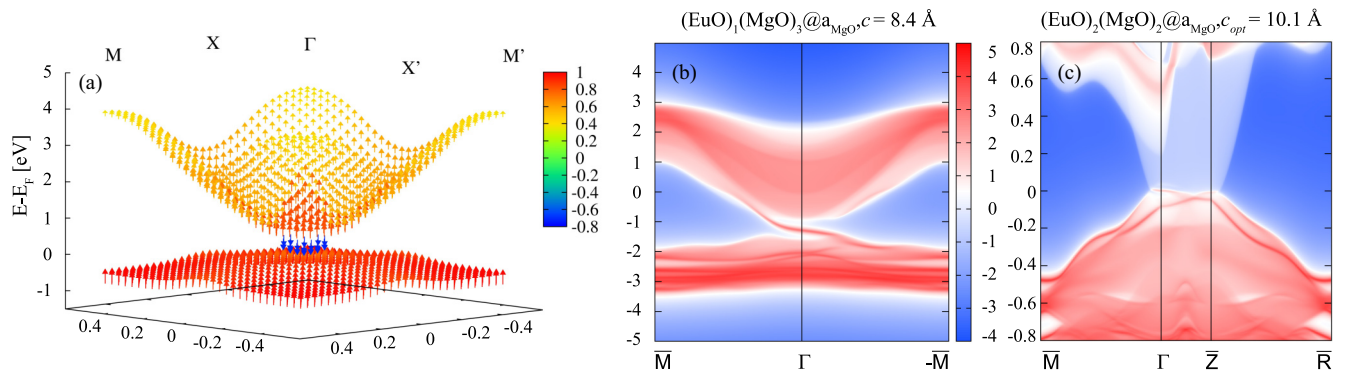


FIG. 5. (a) The band-decomposed spin-texture in k space from the GGA+ U +SOC calculation with magnetization along $[001]$ for the topmost occupied and lowest unoccupied bands [cf. Fig. 4(a)] of the FM $(\text{EuO})_1/(\text{MgO})_3(001)$ superlattice. The color scale denotes the projection on the \hat{z} axis with red (blue) indicating parallel (antiparallel) orientation. (b) edge states for $(\text{EuO})_1/(\text{MgO})_3(001)$ and (c) $(\text{EuO})_2/(\text{MgO})_2(001)$. Red/white represent higher local DOS, blue regions denote the bulk energy gap and red lines mark the edge state connecting the valence and conduction band.

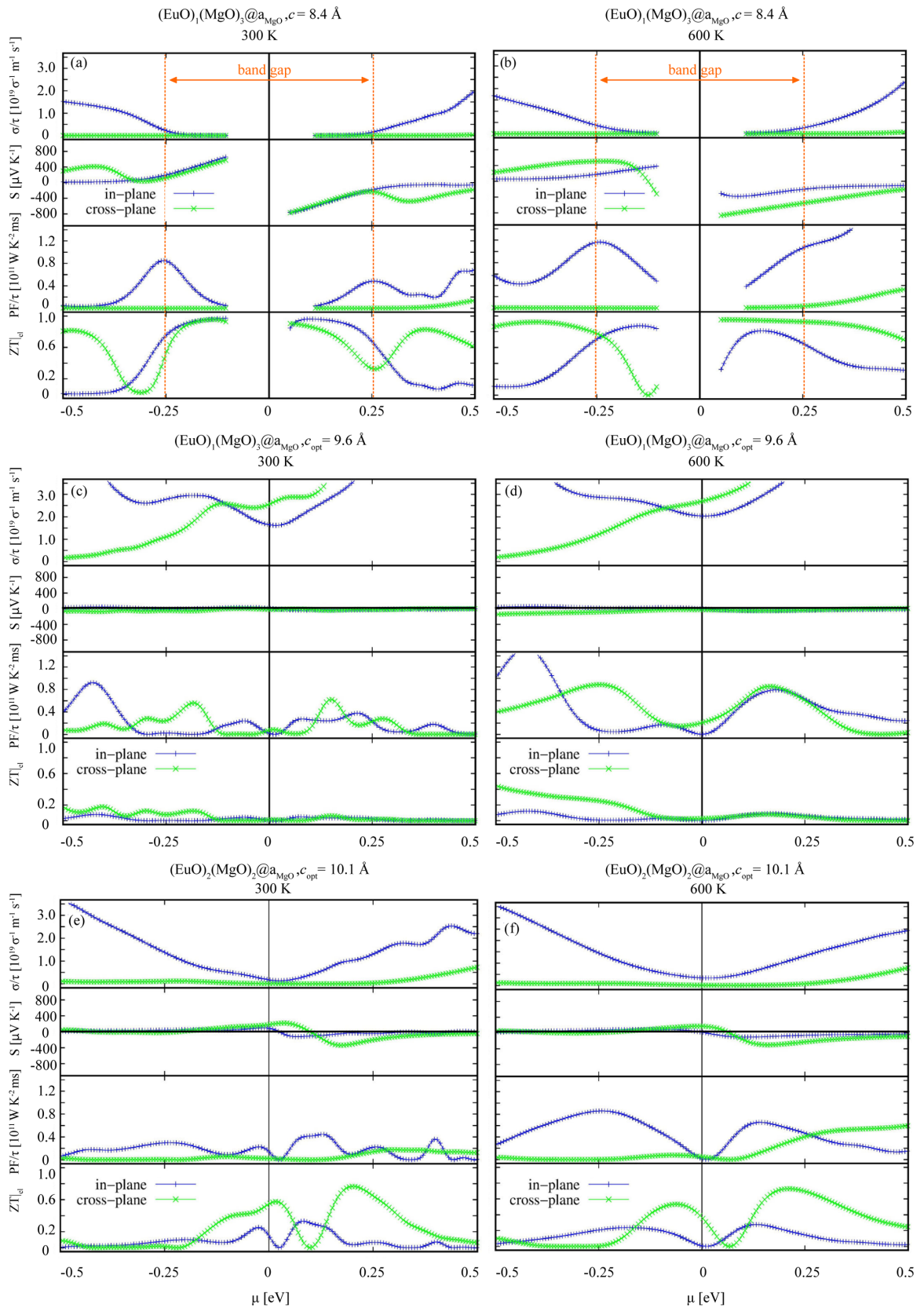


FIG. 6. The in- and cross-plane components of the electrical conductivity tensor divided by the relaxation time τ , the Seebeck coefficient, PF/τ and the electronic contribution to the figure of merit $ZT|_{el}$ are shown as a function of the chemical potential in (a), (b) at 300 K and 600 K for FM $(\text{EuO})_1/(\text{MgO})_3(001)$ superlattice at $c = 8.4 \text{ \AA}$, whereas (c), (d) show the thermoelectric properties with the optimized out-of-plane parameter of $c_{opt} = 9.6 \text{ \AA}$, and (e), (f) the thermoelectric performance of $(\text{EuO})_2/(\text{MgO})_2(001)$ SL.

moment of the conductivity distribution. This tensorial quantity is calculated with the BoltzTraP code [72] as an integral over the transmission using the Fermi distribution. Another quantity connected to the TE performance is the power factor (PF) $PF = S^2\sigma$.

In Fig. 6 we plot σ/τ , the Seebeck coefficient, PF/τ and the electronic contribution to the figure of merit for the systems studied in Fig. 3 at two different temperatures, 300 and 600 K. We recall that $(\text{EuO})_1/(\text{MgO})_3(001)$ with $c = 8.4 \text{ \AA}$ is a Chern insulator upon inclusion of SOC [cf. Figs. 6(a) and 6(b)], while the other two systems remain metallic or semimetallic [see Figs. 6(c)–6(f)]. This is reflected in the vanishing out-of-plane conductivity for the former, whereas the more dispersive bands of $(\text{EuO})_1/(\text{MgO})_3(001)$ with relaxed c lead to higher σ/τ . On the other hand, the flat touching bands along Γ -Z in $(\text{EuO})_2/(\text{MgO})_2(001)$ result in a vanishing out-of-plane conductivity. The Chern insulating system $(\text{EuO})_1/(\text{MgO})_3(001)$ exhibits a much higher Seebeck coefficient, reaching values between 400–800 μVK^{-1} and PF/τ of 0.8×10^{11} (300 K) and $1.2 \times 10^{11} \text{ W/K}^2\text{ms}$ (600 K). The electronic figure of merit $ZT|_{el}$ attains in- and out-of-plane values of ~ 0.8 and ~ 0.5 at 300 K and ~ 0.8 and ~ 0.7 at 600 K at the valence band edge. The corresponding values at the conduction band edge are ~ 0.4 and ~ 0.6 at 300 K and ~ 0.9 and ~ 0.7 at 600 K. In contrast, S , PF/τ and the electronic figure of merit $ZT|_{el}$ are much lower for the metallic case with optimized c . On the other hand, $(\text{EuO})_2/(\text{MgO})_2(001)$ SL exhibits significant values for S ($\sim 200 \mu\text{VK}^{-1}$), PF/τ ($0.8 \cdot 10^{11} \text{ W/K}^2\text{ms}$ at 600 K) and $ZT|_{el}$ (~ 0.6).

Thus, both systems with topologically nontrivial bands and in particular the Chern insulating phase show promising TE properties. The improved performance is associated with the simultaneous presence of flat bands along Γ -Z due to the SOC-induced band inversion and dispersive bands, e.g., along Γ -M. While the former lead to a steep increase of DOS at the band edges, thereby enhancing S , the latter contribute to the electrical conductivity. As mentioned above, we consider here only the electronic contribution to the thermal conductivity, however, we expect that the high atomic number of Eu (63) and the phonon scattering at interfaces in this layered structure will be beneficial to reduce the lattice contribution to κ .

IV. SUMMARY

In summary, the effect of confinement and strain on the topological and thermoelectric properties of $(\text{EuO})_n/(\text{MgO})_m(001)$ superlattices has been studied by DFT + U + SOC calculations in conjunction with semiclassical

Boltzmann transport theory. Combining two topologically trivial insulators EuO and MgO in a QW structure results in a semimetallic phase for $(\text{EuO})_1/(\text{MgO})_3(001)$ SL when the lattice parameters are constrained to the ones of MgO. The inclusion of SOC opens a substantial band gap of 0.51 eV due to a band inversion between Eu 4*f* and 5*d* bands. This mechanism is distinct to the ones in EuO/CdO [33] and EuO/GdN SLs [34], where the band inversion takes place between bands of different elements in the two constituents: Eu 4*f* and Cd 5*s* or Gd 5*d*, respectively. The resulting Chern insulating phase with $C = -1$ shows a sign reversal of the out-of-plane spin components s_z along the loop of band inversion around Γ and a single chiral edge state. A similar band inversion occurs also in $(\text{EuO})_2/(\text{MgO})_2(001)$ SL but with a vanishing band gap. The resulting band rearrangement close to E_F leads to sharp peaks of the Berry curvature at the avoided band crossing close to Γ and Z and a plateau in the anomalous Hall conductivity below E_F with a notable value of $-1.04 e^2/h$.

Moreover, the $(\text{EuO})_1/(\text{MgO})_3(001)$ SL at the MgO lattice parameter exhibits enhanced thermoelectric performance in terms of Seebeck coefficient of 400–800 μVK^{-1} and PF/τ of 0.8 – $1.2 \cdot 10^{11} \text{ W/K}^2\text{ms}$ and an electronic figure of merit of 0.4–0.9 at the band edges depending on temperature, driven by the confinement and the topological nature of the system. Similarly, an out-of-plane electronic ZT of 0.6 is achievable in $(\text{EuO})_2/(\text{MgO})_2(001)$ SL. The opening of a gap due to SOC-driven band inversion with steep increase of DOS at the band edges due to the flatness of bands along the Γ -Z direction promotes high values of the Seebeck coefficient and PF, whereas concomitant dispersive bands contribute to the electrical conductivity. A similar enhanced thermoelectric performance was found in other oxide heterostructures at the verge of a metal-to-insulator transition (though not of topological nature) [45,48]. The results presented here establish a link between topological and thermoelectric properties, in particular for systems with broken inversion symmetry.

ACKNOWLEDGMENTS

We acknowledge useful discussions with M. Müller and A. Lorke on EuO/MgO quantum wells and funding by the German Research Foundation (DFG) within CRC/TRR80 (Project No. 107745057, subproject G3) and CRC1242 (Project No. 278162697, subproject C02) and computational time at the Leibniz Rechenzentrum Garching, project pr87ro. We also would like to thank G. Kämmerer for performing initial calculations with Wien2k.

- [1] X. L. Qi and S. C. Zhang, *Phys. Today* **63**(1), 33 (2010).
 [2] M. Z. Hasan and C. L. Kane, *Rev. Mod. Phys.* **82**, 3045 (2010).
 [3] J. Moore, *Nature (London)* **464**, 194 (2010).
 [4] X. L. Qi and S. C. Zhang, *Rev. Mod. Phys.* **83**, 1057 (2011).
 [5] H. Zhang, C.-X. Liu, X.-L. Qi, X. Dai, Z. Fang, and S.-C. Zhang, *Nat. Phys.* **5**, 438 (2009).

- [6] D. Hsieh, Y. Xia, D. Qian, L. Wray, F. Meier, J. H. Dil, J. Osterwalder, L. Patthey, A. V. Fedorov, H. Lin, A. Bansil, D. Grauer, Y. S. Hor, R. J. Cava, and M. Z. Hasan, *Phys. Rev. Lett.* **103**, 146401 (2009).
 [7] Y. L. Chen, J. G. Analytis, J.-H. Chu, Z. K. Liu, S.-K. Mo, X. L. Qi, H. J. Zhang, D. H. Lu, X. Dai, Z. Fang, S. C. Zhang, I. R. Fisher, Z. Hussain, and Z.-X. Shen, *Science* **325**, 178 (2009).

- [8] J. Zhang, C.-Z. Chang, Z. Zhang, J. Wen, X. Feng, K. Li, M. Liu, K. He, L. Wang, X. Chen, Q.-K. Xue, X. Ma, and Y. Wang, *Nat. Commun.* **2**, 574 (2011).
- [9] L. Muchler, F. Casper, B. Yan, S. Chadov, and C. Felser, *Phys. Status Solidi RRL* **7**, 91 (2013).
- [10] N. Xu, Y. Xu, and J. Zhu, *npj Quantum Mater.* **2**, 51 (2017).
- [11] H. Weng, R. Yu, X. Hu, X. Dai, and Z. Fang, *Adv. Phys.* **64**, 227 (2015).
- [12] Y. Ren, Z. Qiao, and Q. Niu, *Rep. Prog. Phys.* **79**, 066501 (2016).
- [13] C.-X. Liu, X.-L. Qi, X. Dai, Z. Fang, and S.-C. Zhang, *Phys. Rev. Lett.* **101**, 146802 (2008).
- [14] R. Yu, W. Zhang, H.-J. Zhang, S.-C. Zhang, X. Dai, and Z. Fang, *Science* **329**, 61 (2010).
- [15] C. Fang, M. J. Gilbert, and B. A. Bernevig, *Phys. Rev. Lett.* **112**, 046801 (2014).
- [16] H. Zhang, C. Lazo, S. Blugel, S. Heinze, and Y. Mokrousov, *Phys. Rev. Lett.* **108**, 056802 (2012).
- [17] M. Zhou, Z. Liu, W. Ming, Z. Wang, and F. Liu, *Phys. Rev. Lett.* **113**, 236802 (2014).
- [18] X.-L. Sheng and B. K. Nikolic, *Phys. Rev. B* **95**, 201402(R) (2017).
- [19] F. D. M. Haldane, *Phys. Rev. Lett.* **61**, 2015 (1988).
- [20] D. Xiao, W. Zhu, Y. Ran, N. Nagaosa, and S. Okamoto, *Nat. Commun.* **2**, 596 (2011).
- [21] J. L. Lado, V. Pardo, and D. Baldomir, *Phys. Rev. B* **88**, 155119 (2013).
- [22] S. Okamoto, W. Zhu, Y. Nomura, R. Arita, D. Xiao, and N. Nagaosa, *Phys. Rev. B* **89**, 195121 (2014).
- [23] D. Doennig, S. Baidya, W. E. Pickett, and R. Pentcheva, *Phys. Rev. B* **93**, 165145 (2016).
- [24] H. Guo, S. Gangopadhyay, O. Kksal, R. Pentcheva, and W. E. Pickett, *npj Quantum Mater.* **2**, 4 (2017).
- [25] H. S. Lu and G. Y. Guo, *Phys. Rev. B* **99**, 104405 (2019).
- [26] O. Kksal and R. Pentcheva, *Sci. Rep.* **9**, 17306 (2019).
- [27] O. Kksal, S. Baidya, and R. Pentcheva, *Phys. Rev. B* **97**, 035126 (2018).
- [28] O. Kksal and R. Pentcheva, *J. Phys. Chem. Solids* **128**, 301 (2019).
- [29] H. Huang, Z. Liu, H. Zhang, W. Duan, and D. Vanderbilt, *Phys. Rev. B* **92**, 161115(R) (2015).
- [30] T. Cai, X. Li, F. Wang, S. Ju, J. Feng, and C.-D. Gong, *Nano Lett.* **15**, 6434 (2015).
- [31] J. L. Lado, D. Guterding, P. Barone, R. Valenti, and V. Pardo, *Phys. Rev. B* **94**, 235111 (2016).
- [32] G. A. Fiete and A. Ruegg, *J. Appl. Phys.* **117**, 172602 (2015).
- [33] H. Zhang, J. Wang, G. Xu, Y. Xu, and S.-C. Zhang, *Phys. Rev. Lett.* **112**, 096804 (2014).
- [34] K. F. Garrity and D. Vanderbilt, *Phys. Rev. B* **90**, 121103(R) (2014).
- [35] B. A. Bernevig and S. C. Zhang, *Phys. Rev. Lett.* **96**, 106802 (2006).
- [36] B. A. Bernevig, T. L. Hughes, and S. C. Zhang, *Science* **314**, 1757 (2006).
- [37] M. Knig, S. Wiedmann, C. Brune, A. Roth, H. Buhmann, L. W. Molenkamp, X.-L. Qi, and S. C. Zhang, *Science* **318**, 766 (2007).
- [38] A. Mauger and C. Godart, *Phys. Rep.* **141**, 51 (1986).
- [39] S. G. Altendorf, A. Efimenko, V. Oliana, H. Kierspel, A. D. Rata, and L. H. Tjeng, *Phys. Rev. B* **84**, 155442 (2011).
- [40] R. Sutarto, S. G. Altendorf, B. Coloru, M. Moretti Sala, T. Haupricht, C. F. Chang, Z. Hu, C. Schubler-Langeheine, N. Hollmann, H. Kierspel, H. H. Hsieh, H.-J. Lin, C. T. Chen, and L. H. Tjeng, *Phys. Rev. B* **79**, 205318 (2009).
- [41] C. Caspers, A. Gloskovskij, W. Drube, C. M. Schneider, and M. Muller, *Phys. Rev. B* **88**, 245302 (2013).
- [42] G. M. Prinz, T. Gerber, A. Lorke, and M. Muller, *Appl. Phys. Lett.* **109**, 202401 (2016).
- [43] L. D. Hicks, T. C. Harman, and M. S. Dresselhaus, *Appl. Phys. Lett.* **63**, 3230 (1993).
- [44] H. Ohta, S. Kim, Y. Mune, T. Mizoguchi, K. Nomura, S. Ohta, T. Nomura, Y. Nakanishi, Y. Ikuhara, M. Hirano, H. Hosono, and K. Koumoto, *Nat. Mater.* **6**, 129 (2007).
- [45] B. Geisler and R. Pentcheva, *Phys. Rev. Mater.* **2**, 055403 (2018).
- [46] B. Geisler and R. Pentcheva, *Phys. Rev. Appl.* **11**, 044047 (2019).
- [47] F. Belviso, V. E. P. Claerbout, A. Comas-Vives, N. S. Dalal, F.-R. Fan, A. Filippetti, V. Fiorentini, L. Foppa, C. Franchini, B. Geisler, L. M. Ghiringhelli, A. Gro, S. Hu, J. niguez, S. K. Kauwe, J. L. Musfeldt, P. Nicolini, R. Pentcheva, T. Polcar, W. Ren *et al.*, *Inorg. Chem.* **58**, 14939 (2019).
- [48] M. Verma, B. Geisler, and R. Pentcheva, *Phys. Rev. B* **100**, 165126 (2019).
- [49] I. Pallecchi, F. Telesio, D. Li, A. Fete, S. Gariglio, J.-M. Triscone, A. Filippetti, P. Delugas, V. Fiorentini, and D. Marr, *Nat. Commun.* **6**, 6678 (2015).
- [50] A. Filippetti, P. Delugas, M. J. Verstraete, I. Pallecchi, A. Gadaleta, D. Marr, D. F. Li, S. Gariglio, and V. Fiorentini, *Phys. Rev. B* **86**, 195301 (2012).
- [51] P. Delugas, A. Filippetti, M. J. Verstraete, I. Pallecchi, D. Marr, and V. Fiorentini, *Phys. Rev. B* **88**, 045310 (2013).
- [52] D. I. Bilc, C. G. Floare, L. P. Zrbo, S. Garabagiu, S. Lemal, and P. Ghosez, *J. Phys. Chem. C* **120**, 25678 (2016).
- [53] G. Kresse and D. Joubert, *Phys. Rev. B* **59**, 1758 (1999).
- [54] G. Kresse and J. Furthmuller, *Phys. Rev. B* **54**, 11169 (1996).
- [55] J. P. Perdew, K. Burke, and M. Ernzerhof, *Phys. Rev. Lett.* **77**, 3865 (1996).
- [56] P. E. Blchl, O. Jepsen, and O. K. Andersen, *Phys. Rev. B* **49**, 16223 (1994).
- [57] A. I. Liechtenstein, V. I. Anisimov, and J. Zaanen, *Phys. Rev. B* **52**, R5467(R) (1995).
- [58] P. Larson and W. R. L. Lambrecht, *J. Phys.: Condens. Matter* **18**, 11333 (2006).
- [59] P. Larson and W. R. L. Lambrecht, *Phys. Rev. B* **74**, 085108 (2006).
- [60] M. Schlipf, M. Betzinger, M. Lezai, C. Friedrich, and S. Blugel, *Phys. Rev. B* **88**, 094433 (2013).
- [61] W. Y. Tong, H. C. Ding, Y. C. Gao, S. J. Gong, X. Wan, and C. G. Duan, *Phys. Rev. B* **89**, 064404 (2014).
- [62] G. Guntherodt, P. Wachter, and D. M. Imboden, *Phys. kondens. Mater.* **12**, 292 (1971).
- [63] B. T. Matthias, R. M. Bozorth, and J. H. Van Vleck, *Phys. Rev. Lett.* **7**, 160 (1961).
- [64] D. M. Roessler and W. C. Walker, *Phys. Rev.* **159**, 733 (1967).
- [65] P. K. de Boer and R. A. de Groot, *J. Phys.: Condens. Matter* **10**, 10241 (1998).
- [66] Y. Fei, *Am. Mineral.* **84**, 272 (1999).

- [67] R. C. Whited, C. J. Flaten, and W. C. Walker, *Solid State Commun.* **13**, 1903 (1973).
- [68] F. Fuchs, C. Rödl, A. Schleife, and F. Bechstedt, *Phys. Rev. B* **78**, 085103 (2008).
- [69] V. Begum, M. E. Gruner, C. Vorwerk, C. Draxl, and R. Pentcheva, [arXiv:2012.08960](https://arxiv.org/abs/2012.08960).
- [70] K. Schwarz and P. Blaha, *Comput. Mater. Sci.* **28**, 259 (2003).
- [71] A. A. Mostofi, J. R. Yates, Y.-S. Lee, I. Souza, D. Vanderbilt, and N. Marzari, *Comput. Phys. Commun.* **178**, 685 (2008).
- [72] G. K. H. Madsen and D. J. Singh, *Comput. Phys. Commun.* **175**, 67 (2006).
- [73] H. G. Zimmer, K. Takemura, K. Syassen, and K. Fischer, *Phys. Rev. B* **29**, 2350(R) (1984).
- [74] V. Eyert and W. Nolting, *Z. Phys. B* **64**, 341 (1986).
- [75] V. Eyert and W. Nolting, *Solid State Commun.* **60**, 905 (1986).
- [76] Q. Wu, S. Zhang, H. Song, M. Troyer, and A. A. Soluyanov, *Comput. Phys. Commun.* **224**, 405 (2018).